Maximum Likelihood and Suboptimal Schemes for Micro-Doppler Estimation using Carrier Diverse Doppler Radars

Pawan Setlur, Fauzia Ahmad, Moeness Amin
Radar Imaging Lab, Center for Advanced Communications,
Villanova University, Villanova, PA 19085, USA.
E-mail:{pawan.setlur, fauzia.ahmad, moeness.amin}@villanova.edu

Abstract—Carrier diverse radars, known as dual frequency radars, employ two different frequencies, and can be effective in determining the moving target range in urban sensing and through-the-wall radar applications. In this paper, we derive the maximum likelihood (ML) estimator for the micro-Doppler motion parameters from the dual frequency radar returns. Micro-Doppler signatures, which are commonly associated with vibrating, oscillating, and rotating objects, have emerged to be an important tool in target detection and classification. Unlike linear models, the respective ML estimator does not assume a closed form expression. We solve the ML estimator for dual-frequency radar operations by applying an iteratively reweighted nonlinear least squares algorithm (IRNLS), which is initiated using suboptimal solutions. The ML-IRNLS algorithm is applied to both simulated and experimental radar returns for estimating the range and the motion parameters of indoor targets.

Keywords- Doppler radar, carrier diversity, urban sensing, micro-Doppler, maximum likelihood.

I. INTRODUCTION

Urban sensing and through-the-wall radar imaging address the desire to detect, locate, and classify both animate and inanimate targets [1]-[4]. Range estimation is typically performed by linear frequency modulated radars, pulse compression radars, or pulse Doppler radars [5]. Such radar systems are wideband so as to meet the range resolution requirements. However, the operational logistics and system requirements for urban sensing, such as cost, hardware complexity, and portability, may impede or prohibit the use of such radar systems. Further, bandwidth allocation issues may arise since radio frequency (RF) penetration through the walls follows a lowpass filtering model with typical cutoff in the low GHz range, where much of the RF spectrum may be jammed or taken over, in part or fully by adversaries or other emitters. On the other hand, a dual-frequency approach for target range estimation, combined with wide array aperture, can meet the requirements of different system operation modes, and is likely to emerge as the preferred approach in most urban sensing and rescue missions [1],[6]. The dual frequency or carrier diversity is induced by using two different carrier frequencies which are selected to achieve a desirable maximum unambiguous range. The latter is important to allow a unique range estimate of a target, and should be based on the *a priori* knowledge (possible through aerial mapping or ground access) of the spatial extent of the urban structure under surveillance. The technique of employing two frequencies to estimate range has been used in many other radar applications [7], [8].

In this paper, we apply a dual frequency radar for target range and parameter estimation. We consider the micro-Doppler (MD) target motion profile [9]. Micro-Doppler analysis has been used in many applications for human gait analysis, multistatic radar applications, etc., such works can be seen for example in [10], [11], and references therein. RF signatures of indoor inanimate objects, such as fans, vibrating machineries, and clock pendulums, and animate objects, like the limbs in human gait are characterized by MD motion. Translational motions, producing constant velocity or accelerating velocity, respectively produce complex sinusoids and linear frequency modulation to the incident waveform. The ML techniques for parameter estimation of such returns has been treated in [12], [13], and references

therein. However, the ML for micro Doppler, which gives rise to sinusoidal FM signals, has not yet been examined and is the subject of this paper. We derive the maximum likelihood optimal estimator for MD motion parameters. The results are compared with the Cramér-Rao lower bounds (CRBs) for MD motion parameters which were recently derived in [14] for dual-frequency operations.

We consider a single moving target whose MD motion profile can be modeled by a finite number of parameters. The MD is further classified as rotational or vibrational MD based on radar cross section (RCS) fluctuations. Maximum likelihood (ML) technique for motion parameter estimation is then formulated and solved using step wise concentration to obtain an iteratively reweighted least squares algorithm. The iterative algorithm is initialized using suboptimal estimates and applied to real radar returns to obtain ML estimates of the MD parameters. It is noted that the focus of this paper is on single antenna operation. For a multiple target scene, assuming that the targets are separable in cross-range and spatial processing (beamforming) is used in conjunction with the dual-frequency radar, the ML analysis presented in this paper is applicable to each individual separated target return.

A brief outline of the paper is as follows. Section II describes the signal model. In Sections III and IV, we discuss, respectively, the ML and suboptimal estimation schemes for the micro-Doppler motions. Section V contains the simulation and experimental results, followed by the conclusions in Section VI.

II. SIGNAL MODEL

The signal returns for the dual frequency Doppler radar after down conversion to baseband and using N samples are given by,

$$x_i(n) = s_i(n) + v_i(n) = h_i(n;\boldsymbol{\psi}')\exp\left(j\frac{4\pi f_i}{c}R(n;\boldsymbol{\psi})\right) + v_i(n), \quad i=1,\ 2, \text{ and } n=0,1,\ldots,N-1$$
$$E\left\{v_1(n)v_2^{*}(k)\right\}=0 \ \ \forall n,k; \quad E\left\{v_i(n)v_i^{*}(k)\right\}=0 \ \ \forall n\neq k,\ i=1,2, E\left\{v_i(n)v_i^{*}(k)\right\}=\sigma_i^2 \ \ \forall n=k,\ i=1,2 \tag{1}$$

where f_i, $i=1,2$ are the carrier frequencies, c is the speed of light in free space, and the superscript '$*$' denotes the complex conjugate operation. The target range, $R(n;\boldsymbol{\psi})$, is parameterized by a vector $\boldsymbol{\psi}\in\Re^{P\times 1}$ of P desired parameters. The amplitude $h_i(n;\boldsymbol{\psi}')$, measured at the i-th frequency, captures the

time variations in the target RCS, and is a function of a subset $\boldsymbol{\psi}'$ of the parameter vector $\boldsymbol{\psi}$. The noise, $v_1(\cdot)$ and $v_2(\cdot)$, at the two carrier frequencies, are assumed to be complex circular AWGN and uncorrelated. Further, the noise sequences are i.i.d for each carrier frequency. Note that the model in (1) corresponds to the discrete-time equivalent of the continuous-time signals, i.e., $x_i(n) = x_i(nT_s)$, where T_s is the sampling period and has been suppressed in the notations for convenience. The returns in (1) can be statistically characterized by a multivariate complex Gaussian probability density function (pdf), $p(\mathbf{x};\mathbf{s})$,

$$p(\mathbf{x};\mathbf{s}) = \frac{1}{\pi^{2N}\det(\mathbf{C})}\exp(-(\mathbf{x}-\boldsymbol{\mu})^H \mathbf{C}^{-1}(\mathbf{x}-\boldsymbol{\mu})) \tag{2}$$

where the received signals at the two frequencies are appended to form a long vector,

$$\begin{aligned}
\mathbf{x} &= \mathbf{s} + \mathbf{v} = \left[x_1(0), x_1(1), \ldots, x_1(N-1), x_2(0), x_2(1), \ldots, x_2(N-1)\right]^T = [\mathbf{x_1} \quad \mathbf{x_2}]^T \\
\mathbf{s} &= [s_1(0), s_1(1), \ldots, s_1(N-1), s_2(0), s_2(1), \ldots, s_2(N-1)]^T = [\mathbf{s_1} \quad \mathbf{s_2}]^T \\
\mathbf{v} &= [v_1(0), v_1(1), \ldots, v_1(N-1), v_2(0), v_2(1), \ldots, v_2(N-1)]^T = [\mathbf{v_1} \quad \mathbf{v_2}]^T
\end{aligned} \tag{3}$$

The mean $\boldsymbol{\mu} = E\{\mathbf{x}\}$ equals $[\mathbf{s_1} \quad \mathbf{s_2}]^T$ and the covariance matrix $\mathbf{C}$ is Hermitian with the following diagonal structure,

$$\mathbf{C} = E\{(\mathbf{x}-\boldsymbol{\mu})(\mathbf{x}-\boldsymbol{\mu})^H\} = \begin{bmatrix} \sigma_1^2\mathbf{I} & \mathbf{0}_{N\times N} \\ \mathbf{0}_{N\times N} & \sigma_2^2\mathbf{I} \end{bmatrix} \tag{4}$$

where $\mathbf{I}$ is an identity matrix of dimensions $N \times N$.

III. MAXIMUM LIKELIHOOD ESTIMATION

We consider the noise free return $\mathbf{s}$, which is a function of $R(n;\boldsymbol{\psi})$, $h_i(n;\boldsymbol{\psi}')$, and f_i, $i = 1, 2$, to be parameterized by the vector $\boldsymbol{\psi}$ of P desired parameters. Hereafter, for notational succinctness, we denote $\mathbf{s} = \mathbf{s}(\boldsymbol{\psi})$. The ML estimator for $\boldsymbol{\psi} = [\psi_1, \ \psi_2, \ \psi_3 ..... \psi_P]^T$ is defined as [15],

$$\hat{\boldsymbol{\psi}} = \arg\max_{\boldsymbol{\psi}} p(\mathbf{x}; s(\boldsymbol{\psi})) = \arg\max_{\boldsymbol{\psi}} \ \ln(p(\mathbf{x}; s(\boldsymbol{\psi}))) \tag{5}$$

If the elements of the covariance matrix, i.e., σ_i^2, $i=1,\ 2$, are unknown, then using (2) and ignoring the constant terms, the ML estimator of the complete parameter vector, $\boldsymbol{\theta}=[\boldsymbol{\psi}^T, \sigma_1^2,\ \sigma_2^2]^T$ can be expressed as,

$$\hat{\boldsymbol{\theta}} = \arg\max_{\boldsymbol{\theta}} \left(-N\ln(\sigma_1^2) - N\ln(\sigma_2^2) - \frac{\left\|\mathbf{x}_1 - \mathbf{s}_1(\boldsymbol{\psi})\right\|^2}{\sigma_1^2} - \frac{\left\|\mathbf{x}_2 - \mathbf{s}_2(\boldsymbol{\psi})\right\|^2}{\sigma_2^2} \right) \tag{6}$$

Computing the log likelihood (LL) score with respect to the noise nuisance parameters σ_i^2, $i=1,\ 2$, and equating it to zero, we obtain

$$\sigma_i^2 = \frac{\left\|\mathbf{x}_i - \mathbf{s}_i(\boldsymbol{\psi})\right\|^2}{N}, \quad \text{for } i=1,\ 2 \tag{7}$$

Concentrating the LL with respect to σ_i^2, i.e., substituting (7) in (6), yields

$$\hat{\boldsymbol{\psi}} = \arg\max_{\boldsymbol{\psi}} \left(-N\ln\left(\frac{\left\|\mathbf{x}_1 - \mathbf{s}_1(\boldsymbol{\psi})\right\|^2}{N} \times \frac{\left\|\mathbf{x}_2 - \mathbf{s}_2(\boldsymbol{\psi})\right\|^2}{N} \right) \right) = \arg\min_{\boldsymbol{\psi}} \ln\left(\prod_{i=1}^{2} \frac{\left\|\mathbf{x}_i - \mathbf{s}_i(\boldsymbol{\psi})\right\|^2}{N} \right) \tag{8a}$$

$$\hat{\sigma}_i^2 = \frac{\left\|\mathbf{x}_i - \mathbf{s}_i(\hat{\boldsymbol{\psi}})\right\|^2}{N} \tag{8b}$$

The ML estimator for the noise nuisance parameters is provided in (8b), and is the same as the expression in (7) with $\boldsymbol{\psi}$ replaced by $\hat{\boldsymbol{\psi}}$. Notice that the noise estimate at one frequency only depends on the data measured at the same frequency. However, it also depends on the ML parameter estimates obtained from the combined frequency information, and as such, the problem cannot be decoupled into two separate ML parts, each corresponding to a single frequency. Equation 8(a, b) constitutes the ML estimator for the dual frequency radar, and due to the involvement of the two terms, it does not have a closed form solution. If the elements of the covariance matrix $\mathbf{C}$ are known, the ML estimator for $\boldsymbol{\psi}$ takes the form

$$\hat{\boldsymbol{\psi}} = \arg\min_{\boldsymbol{\psi}} \ (\mathbf{x} - \mathbf{s}(\boldsymbol{\psi}))^H \mathbf{C}^{-1} (\mathbf{x} - \mathbf{s}(\boldsymbol{\psi})) = \arg\min_{\boldsymbol{\psi}} \left(\frac{\left\|\mathbf{x}_1 - \mathbf{s}_1(\boldsymbol{\psi})\right\|^2}{\sigma_1^2} + \frac{\left\|\mathbf{x}_2 - \mathbf{s}_2(\boldsymbol{\psi})\right\|^2}{\sigma_2^2} \right) \tag{9}$$

The step wise concentration approach can be applied using (9) to provide an iterative solution to 8(a,b). The iterative ML algorithm is formulated as follows.

1. Initialize with $\mathbf{C}_0 = \mathbf{I}$, where $\mathbf{I}$ is an identity matrix of the same dimension as $\mathbf{C}_0$.

2. Using (9), find the estimate $\hat{\boldsymbol{\psi}}_0$ of $\boldsymbol{\psi}$.

3. Use $\hat{\boldsymbol{\psi}}_0$ in (8b) to obtain the noise variance estimates $\hat{\sigma}_{i1}^2 = \left\|\mathbf{x}_i - \mathbf{s}_i(\hat{\boldsymbol{\psi}}_0)\right\|^2 / N$, and construct the covariance matrix $\mathbf{C}_1 = Diag\ [\hat{\sigma}_{11}^2 \times \mathbf{1}, \hat{\sigma}_{21}^2 \times \mathbf{1}]$, where the operator $Diag[\cdot]$ transforms a vector into a diagonal matrix and $\mathbf{1} = [1,1,1..1]_{1\times N}$.

4. Recursively solve at the kth iteration $(k > 1)$,

$$\hat{\boldsymbol{\psi}}_k = \arg\min_{\boldsymbol{\psi}} \ (\mathbf{x} - s(\boldsymbol{\psi}))^H \mathbf{C}_k^{-1} (\mathbf{x} - s(\boldsymbol{\psi})), \quad \text{initialized with } \hat{\boldsymbol{\psi}}_{k-1}$$
$$\hat{\sigma}_{i(k+1)}^2 = \left\|\mathbf{x}_i - \mathbf{s}_i(\hat{\boldsymbol{\psi}}_k)\right\|^2 / N, \ \forall i = 1,2 \ ; \ \mathbf{C}_{(k+1)} := Diag[\hat{\sigma}_{1(k+1)}^2 \times \mathbf{1}, \hat{\sigma}_{2(k+1)}^2 \times \mathbf{1}] \tag{10}$$

5. Stop at convergence, or when an appropriate terminating criterion is satisfied.

The solution of step 4 depends on the underlying motion model, as delineated next. We note that the estimate $\hat{\boldsymbol{\psi}}_0$ is the non-linear least squares (NLS) estimate. Further, in step 4, the covariance matrix $\mathbf{C}_k$ is not stressed to be an estimate for reasons to follow shortly. As evident from the above iterative ML implementation, the step-wise concentration approach does not treat the noise variances as of known or estimated values, but rather alternates between the two assumed hypotheses. In other words, for every iteration, a quasi-ML objective is optimized. The step-wise algorithm has been used in generalized linear models in statistical literature [16] and in robust statistics for M-estimation [17]. It is often described as the iteratively reweighted least squares (IRLS). The "reweighting" at each iteration occurs in the estimation of $\hat{\boldsymbol{\psi}}_k$ through a known $\mathbf{C}_k$, as seen in (10). However, for the problem at hand, as shown in the following section, $\mathbf{s}(\boldsymbol{\psi})$ is nonlinear, and hence a more appropriate name for the algorithm would be the iteratively reweighted nonlinear least squares (IRNLS). Henceforth, we will refer to the iterative ML algorithm as IRNLS. Proof of convergence of the IRNLS estimates is provided in the Appendix.

Three terminating criteria may be considered for the IRNLS algorithm. Denoting the negative LL cost by $\ell(\boldsymbol{\psi})$, an appropriate criterion is when $\ell(\hat{\boldsymbol{\psi}}_k) - \ell(\hat{\boldsymbol{\psi}}_{k-1}) \le \dot{\varepsilon}$, where $\dot{\varepsilon}$ is an arbitrarily small user-

defined positive constant, in which case $\hat{\boldsymbol{\psi}}_k$ will be the final ML estimate. Another terminating criterion could be $\left\|\hat{\boldsymbol{\psi}}_k - \hat{\boldsymbol{\psi}}_{k-1}\right\| \le \ddot{\varepsilon}$, where $\ddot{\varepsilon}$ is the available machine precision or can be user-defined. The third terminating criterion is simply constraining the maximum number of iterations, i.e., iterate (10) until $k = k_{\max}$. We use this criterion in the simulations. A general flowchart of the ML algorithm is shown in Fig. 1.

In the following, we associate $\mathbf{s}(\boldsymbol{\psi})$ to different MD motion profiles, and use the IRNLS to derive the respective optimal ML solution.

A. Micro-Doppler

The MD returns can be classified as a) vibrational MD and b) rotational MD. Although the phase of the returns is identical in both cases, a difference between the two exists in terms of the amplitude or RCS fluctuations.

A.1 Vibrational MD

The vibrational MD arises due to vibrations of the scatterers on the target or of the target itself, example being a target moving back and forth or undergoing a simple harmonic motion (SHM). The vibrational MD is characterized by a sinusoidal instantaneous frequency. It is parameterized by $\boldsymbol{\psi} = [R_o, d, \omega_o, \varphi_o]$, where R_o is the range of the target at rest or simply the mean range, d is the maximum radial displacement, ω_o is the vibrational frequency, and φ_o is a constant phase. The time-varying range profile for this motion is given by,

$$R(n;\boldsymbol{\psi}) = R_o + d\cos(\omega_o n - \varphi_o) \tag{11}$$

Typical indoor vibrating targets have small displacements relative to the target range, especially for longer radar standoff distances from the wall that are normally used for through-the-wall radar operations. Accordingly, the target aspect angle and hence the RCS is considered constant, thereby yielding a constant amplitude, i.e., $h_i(n;\boldsymbol{\psi}') = \rho_i$, $i = 1, 2$. Substituting the expressions for $h_i(n;\boldsymbol{\psi}')$ and $R(n;\boldsymbol{\psi})$ in (1), we obtain the signal returns as,

$$x_i(n) = \rho_i \exp\left(j\frac{4\pi f_i (R_o + d\cos(\omega_o n - \varphi_o))}{c} \right) + v_i(n),\ \forall i = 1,2 \tag{12}$$

The radar returns in (12) represent sinusoidal FM signals. Using the data vector **x**, comprised of the returns of (12), in (10) defines the IRNLS-ML estimator for the vibrational MD motion profile. The noise-free signal vector **s** can be decomposed into two multiplicative terms, one containing R_o and the other being a function of the remaining parameters in $\boldsymbol{\psi}$. Accordingly, we express the IRNLS-iterations as

$$\begin{gathered}
\hat{\boldsymbol{\psi}}_k = \arg\min_{\boldsymbol{\psi}'} (\mathbf{x} - \mathbf{A}(\boldsymbol{\psi}')\mathbf{b})^H \mathbf{C}_k^{-1} (\mathbf{x} - \mathbf{A}(\boldsymbol{\psi}')\mathbf{b}),\ \ k > 1,\ \textit{initialized with}\ \hat{\boldsymbol{\psi}}_{k-1} \\
\mathbf{a}_i(\boldsymbol{\psi}') := [1, \exp(j4\pi f_i z(1)/c), \ldots, \exp(j4\pi f_i z(N-1)/c)]^T,\ \boldsymbol{\psi}' := [d, \omega_o, \varphi_o]^T \\
z(n) := d\cos(\omega_o n - \varphi_o),\ \ b_i := \rho_i \exp(j4\pi f_i R_o / c), \forall i = 1,2 \\
\mathbf{A}(\boldsymbol{\psi}') = \begin{bmatrix} \mathbf{a}_1(\boldsymbol{\psi}') & \mathbf{0} \\ \mathbf{0} & \mathbf{a}_2(\boldsymbol{\psi}') \end{bmatrix},\ \ \mathbf{b} = [b_1, b_2]^T,\ \ \mathbf{0} = [0,0,\ldots,0]^T_{N\times 1} \\
\hat{\sigma}^2_{i(k+1)} = \left\| \mathbf{x}_i - \hat{\mathbf{a}}_i(\hat{\boldsymbol{\psi}}'_k)\hat{b}_{ik} \right\|^2 / N,\quad \text{for } i = 1,\ 2,
\end{gathered} \tag{13}$$

In (13), $\hat{b}_{ik}$ denotes the estimate $\hat{b}_i$ at the *k*-th iteration. We proceed by minimizing (13) with respect to **b**, in which case one obtains the well known weighted least squares solution, substituting this into (13) we obtain the final estimates of the parameters as,

$$(\hat{d}_k, \hat{\omega}_{ok}, \hat{\varphi}_{o,k}) = \arg\max_{d,\omega_o,\varphi_o} \left(\frac{\left| \sum_{n=0}^{N-1} x_1(n)\exp(-j4\pi f_1 d\cos(\omega_o n - \varphi_o)/c) \right|^2}{\sigma_{1k}^2} + \frac{\left| \sum_{n=0}^{N-1} x_2(n)\exp(-j4\pi f_2 d\cos(\omega_o n - \varphi_o)/c) \right|^2}{\sigma_{2k}^2} \right),\ \ k > 1$$

$$\begin{gathered}
\hat{\mathbf{A}}_k := \mathbf{A}(\hat{\boldsymbol{\psi}}'_k), \hat{\mathbf{b}}_k := \mathbf{b}(\hat{\boldsymbol{\psi}}'_k) = (\hat{\mathbf{A}}_k^H \mathbf{C}_k^{-1} \hat{\mathbf{A}}_k)^{-1} \hat{\mathbf{A}}_k^H \mathbf{C}_k^{-1} \mathbf{x},\quad \hat{R}_{ok} = \frac{\angle(\hat{b}_{2k} \times \hat{b}_{1k}^*)}{4\pi(f_2 - f_1)} c \\
\hat{\rho}_{ik} = \left| \hat{b}_{ik} \right|,\ \hat{\sigma}^2_{i(k+1)} = \left\| \mathbf{x}_i - \hat{\mathbf{a}}_i(\hat{\boldsymbol{\psi}}'_k)\hat{b}_{ik} \right\|^2 / N,\ i = 1,2
\end{gathered} \tag{14}$$

In (14), $\hat{\mathbf{A}}_k$ and $\hat{\mathbf{b}}_k$, respectively, denote the estimates of **A** and **b** in the *k*-th iteration, defined in (13). Similar notational convention follows for the other parameters. The function maximizations in (14) are solved numerically. It is noted in (14) that the range estimate $\hat{R}_{ok}$ is obtained by subtracting the mean

phase estimates at the two carriers and dividing it by the difference of the carrier frequencies. This estimate corresponds to the standard dual-frequency range estimate to avoid the many ambiguous range solutions see [7, pg. 140]. In other words, we are assuming $R_o \in [0, c/2(f_2 - f_1)]$.

A.2 Rotational MD

As the name suggests, targets which are rotating with respect to a fixed location radar follow this model. Unlike the vibration model, the signal returns due to rotation have RCS fluctuations. This is because the radar observes different elevation aspects of the target, thereby inducing a cyclic amplitude modulation in the radar returns. In general, the RCS fluctuations are geometry dependent. For example, the RCS fluctuations are non-existent for a rotating sphere since the sphere is aspect independent, whereas for other complex targets, the RCS fluctuates cyclically. In this paper, we consider the sinc type fluctuation, which corresponds well to a rotating fan blade [18-20]. It must be noted that most of the typical indoor rotating targets are fans, which may either be ceiling mounted, pedestal or table-top. This is primarily the reason for using the sinc model in the underlying application area. As such, the baseband returns at the two carrier frequencies, for a single blade, can be readily shown to be

$$\begin{aligned} x_i(n) &= h_i(n;\boldsymbol{\psi}')\exp\left(j\frac{4\pi f_i(R_o + d\cos(\omega_o n - \varphi_o))}{c}\right) + v_i(n),\ i = 1,2 \\ h_i(n;\boldsymbol{\psi}') &:= \rho_i\gamma_i(n;\boldsymbol{\psi}') = \rho_i \mathrm{sinc}\left(\frac{4\pi f_i d\cos(\omega_o n - \varphi_o)}{c}\right),\ \boldsymbol{\psi}' := [d, \omega_o, \varphi_o]^T \end{aligned} \tag{15}$$

The sinc function in (15) is defined as $\mathrm{sinc}(x) := \sin(x)/x$. From (15), it is noted that the sinc function has a cyclic behavior which depends on the rotational frequency. The rotational frequency, in turn, is also a function of the sampling frequency, and hence the data in (15) must span at least one cycle for any type of processing to be successfully applied to it. Extending the model in (15) to Q blades, the return at the i-th frequency is given by,

$$\begin{aligned} x_i(n) &= \sum_{q=1}^{Q} h_{iq}(n;\boldsymbol{\psi}')\exp\left(j\frac{4\pi f_i(R_o + d\cos(\omega_o n - \varphi_q))}{c}\right) + v_i(n),\ i = 1,2 \\ h_{iq}(n;\boldsymbol{\psi}') &:= \rho_{iq}\gamma_{iq}(n;\boldsymbol{\psi}') = \rho_{iq}\mathrm{sinc}\left(\frac{4\pi f_i d\cos(\omega_o n - \varphi_q)}{c}\right) \end{aligned} \tag{16}$$

The model in (16) is general, in the sense that it assumes the Q blades are different, and thus ρ_{iq} is indexed by q. If the blades possess identical geometry, and no have manufacturing defects, then as a special case $\rho_{iq} = \rho_i,\ \forall q$. Further, assuming that the blades are placed symmetrically around the main rotor, we can express φ_q as

$$\varphi_q = \varphi_o + (q-1)2\pi / Q, \qquad \mathrm{q} = 1,2,\ldots,Q \tag{17}$$

In this case, the radar return from the rotating object has a harmonic structure with harmonic frequencies at $mQ\omega_o, m = 0,\pm 1,\ldots,\infty$ [18-20]. We must note that the RCS, which is strictly positive and real, is determined from the magnitude squared of the noise free returns in (15) and (16). The returns in (16) can be rewritten in a compact vector notation as

$$\begin{aligned}
&\mathbf{x} = [\mathbf{x}_1^T, \mathbf{x}_2^T]^T = \mathbf{A}(\boldsymbol{\psi}')\mathbf{b} \\
&\mathbf{A}(\boldsymbol{\psi}') := \begin{bmatrix} \mathbf{A}_{11}(\boldsymbol{\psi}') & \mathbf{0} \\ \mathbf{0} & \mathbf{A}_{22}(\boldsymbol{\psi}') \end{bmatrix}, \mathbf{b} := [\mathbf{b}_1^T, \mathbf{b}_2^T]^T \\
&\mathbf{b}_i = [b_{i1}, b_{i2}, \ldots., b_{iQ}]^T,\ b_{iq} = \rho_{iq} \exp(j4\pi f_i R_o / c),\ \mathbf{A}_{ii}(\boldsymbol{\psi}') := \left[\mathbf{a}_{i1}(\boldsymbol{\psi}'), \mathbf{a}_{i2}(\boldsymbol{\psi}'), \ldots, \mathbf{a}_{iQ}(\boldsymbol{\psi}')\right],\ i = 1,2 \\
&\mathbf{a}_{iq}(\boldsymbol{\psi}') := \boldsymbol{\gamma}_{iq} \odot \mathbf{g}_{iq},\ \boldsymbol{\gamma}_{iq} := [\gamma_{iq}(0;\boldsymbol{\psi}'), \boldsymbol{\gamma}_{iq}(1;\boldsymbol{\psi}'), \ldots, \boldsymbol{\gamma}_{iq}(N-1;\boldsymbol{\psi}')]^T,\ q = 1,2,\ldots,Q \\
&\mathbf{g}_{iq}(\boldsymbol{\psi}') := [e^{j4\pi f_i d\cos(\varphi_q)/c}, e^{j4\pi f_i d\cos(\omega_o - \varphi_q)/c}, \ldots, e^{j4\pi f_i d\cos(\omega_o(N-1) - \varphi_q)/c}]^T
\end{aligned} \tag{18}$$

In (18), the symbol '$\odot$' denotes the Hadamard product or element-wise product. Following the analysis for vibrational MD case, it can be readily shown that the IRNLS ML for rotational MD at the k^{th} iteration is given by

$$\begin{aligned}
\hat{\boldsymbol{\psi}}'_k &= \arg\max_{\boldsymbol{\psi}'} \mathbf{x}^H \mathbf{P}_k(\boldsymbol{\psi}')\mathbf{C}_k^{-1}\mathbf{x}, \quad \textit{initialized with } \hat{\boldsymbol{\psi}}'_{k-1} \\
\mathbf{P}_k(\boldsymbol{\psi}') &:= \mathbf{A}_k(\mathbf{A}_k^H\mathbf{C}_k^{-1}\mathbf{A}_k)^{-1}\mathbf{A}_k^H\mathbf{C}_k^{-1} \\
\hat{\mathbf{b}}_k &= (\hat{\mathbf{A}}_k^H\mathbf{C}_k^{-1}\hat{\mathbf{A}}_k)^{-1}\hat{\mathbf{A}}_k^H\mathbf{C}_k^{-1}\mathbf{x} = [\hat{\mathbf{b}}_{1k}^T, \hat{\mathbf{b}}_{2k}^T]^T \\
\hat{R}_{ok} &= \mathbf{1}^T \angle(\hat{\mathbf{b}}_{1k}^* \odot \hat{\mathbf{b}}_{2k}) \times \frac{c}{Q4\pi(f_2 - f_1)} \\
\hat{\sigma}^2_{i(k+1)} &= \left\|\mathbf{x}_i - \hat{\mathbf{a}}_i(\hat{\boldsymbol{\psi}}'_k)\hat{b}_{ik}\right\|^2 / N,\ i = 1,2,\ \hat{\rho}_{iq} = \left|\hat{b}_{iq}\right|,\ \forall q
\end{aligned} \tag{19}$$

where $\mathbf{1}$ is column vector of dimensions Q x 1 whose elements are comprised of all ones, and $\mathbf{A}(\boldsymbol{\psi}')$ and $\mathbf{b}$ are defined in (18). In (19), $\hat{\mathbf{A}}_k := \mathbf{A}(\hat{\boldsymbol{\psi}}'_k)$ is the estimate of the matrix $\mathbf{A}_k$. The function

maximizations in (19), as before is carried out numerically. A special arises when the blades are all identical. I.e., $\rho_{iq} = \rho_i,\ \forall q,$ then the IRNLS ML derived thus far still applies, for example in (19), we simply use $\hat{\rho}_i = \mathbf{1}^T \left| \hat{\mathbf{b}}_i \right| / Q$, where the absolute value is taken element-wise. For a single blade return, we can substitute $q = 1$ in (18-19) and proceed with the analysis.

We use the CRBs to compare the mean squared error (MSE) of the ML estimates for both vibrational and rotational MD motions. The elements of the Fisher Information Matrix (FIM) for rotational MD assuming the sinc model are derived in Section. III. The expressions can then be used to numerically evaluate the inverted FIM. The FIM for vibrational MD, derived in [14], is a special case of the rotational MD FIM.

IV. SUBOPTIMAL ESTIMATORS

Iterative non-linear schemes, ML or otherwise, require proper initial estimates for achieving convergence. The non-linear cost functions of (8a) and (9) have multiple local extrema. Therefore, in order to obtain $\hat{\boldsymbol{\psi}}_1$ in step 2 of the IRNLS-ML algorithm, initial estimates, obtained from suboptimal estimators which depend on the noise free returns, $\mathbf{s}_i(\boldsymbol{\psi}),\ i = 1,2,$ can be used. Below, we discuss the suboptimal estimation schemes for both vibrational and rotational MD.

A. Vibrational MD

Ignoring the contribution of noise for the time being, we note that the Fourier spectrum of the return, $x_i(n),\ i = 1,2$ in (12) is not analytic, and consists of infinitely many harmonics weighted by Bessel functions of the first kind [21],

$$X_i(\omega) = 2\pi\rho_i \exp(j4\pi f_i R_o / c) \sum_{m=-\infty}^{m=\infty} j^m J_m(4\pi f_i d / c)\delta(\omega - m\omega_o)\exp(-jm\varphi_o),\ \ \forall i = 1,2 \qquad (20)$$

where $J_m(\cdot)$ is the m^{th} order Bessel function of the first kind. Since the Bessel functions rapidly decrease in magnitude for increasing m, the Fourier transform (20) of the returns in (12) has at the most $m = K$ significant harmonics. The value of K is readily inferred from the spectrum. With this in mind, we

describe below the suboptimal estimation procedure. Since the noise variances are neither required for estimating the parameters suboptimally nor are they essential to start the IRLS iterations, their suboptimal estimates are omitted.

To obtain initial estimates of ω_o, we choose 2*K*+1 peaks of $X_i(\omega)$, $i=1,2$ and form the vector $\mathbf{y}_i=[X_i(\omega_{-K}),X_i(\omega_{-K+1}),\ldots,X_i(0),\ldots,X_i(\omega_{K-1}),X_i(\omega_K)]^T$. The frequencies corresponding to these peaks are stored in a vector $\boldsymbol{\omega}_i$. Since the noise is different for each carrier frequency, different perturbations in the peak frequency locations can occur. Hence, in general, $\boldsymbol{\omega}_1 \neq \boldsymbol{\omega}_2$. The DC value in the Fourier transform is important, since it serves a reference for automatic peak-picking, and therefore it must be included in the vector $\mathbf{y}_i$. The suboptimal estimates $\omega_{oi,subopt}$, $i=1,2,$ for ω_o can be obtained as,

$$\hat{\omega}_{oi,subopt}=\frac{\mathbf{K}^T\boldsymbol{\omega}_i}{(\mathbf{K}^T\mathbf{K})},\ \forall i=1,\ 2,\ \ \mathbf{K}:=[-K,-K+1,\ldots,0,\ldots,K]^T \tag{21}$$

Equation (21) is similar to the least squares estimator proposed in [22, eq. (35)], with subtle differences due to the model choice.

In order to estimate the remaining parameters, albeit suboptimally, one first needs to estimate the amplitude ρ_i. For this purpose, we employ a computationally efficient technique using higher order statistics which was proposed in [22, eq. (50-52)],

$$\hat{\rho}_{i,subopt}=\sqrt[4]{2\left(\frac{1}{N}\sum_{n=0}^{N-1}|x_i(n)|^2\right)^2-\frac{1}{N}\sum_{n=0}^{N-1}|x_i(n)|^4},\ \forall i=1,2 \tag{22}$$

The above equation relies on the higher order moments of the Gaussian random variable, and may not be valid for other types of distributions. The estimation of d_i depends on classifying the signal returns as wideband or narrowband. We consider the wideband case[1]. The suboptimal estimator proposed in [23], and also used in, [22, eq. (38), eq. (40)], and [24] can be applied to obtain the estimate of d_i, $i=1,2$, as

[1] Narrowband case is treated in [22] and is much simpler than the wideband case.

$$\hat{d}_i = \sqrt{\frac{2(\mathbf{y}_i \odot \mathbf{y}_i^*)^T (\mathbf{K} \odot \mathbf{K})}{\rho_i^2 (\mathbf{y}_i^H \mathbf{y}_i)}}, \ \forall i = 1,2 \tag{23}$$

The estimate for R_o is given by,

$$\hat{R}_{o,subopt} = (\angle X_2(0) X_1^*(0)) c / 4\pi (f_2 - f_1)) \tag{24}$$

Indeed, other techniques, based on (20), can be considered for estimating R_o. However, the suboptimal estimates of (24) were found to perform reasonably well in terms of the mean square error. For φ_o, we use the LS estimator proposed in [22] after appropriately demodulating the phase estimates for R_o.

$$\hat{\varphi}_{oi,subopt} = \frac{-\mathbf{K}^T \arg(\mathbf{y}_i \exp(-j4\pi f_i \hat{R}_{o,subopt} / c))}{\|\mathbf{K}\|^2}, \ \forall i = 1,2 \tag{25}$$

In (25), $\arg(\cdot)$ is the unwrapped phase operator, which operates element-wise on a vector. We note that the suboptimal techniques for vibrational MD rely heavily on peak picking in the discrete Fourier transform of the returns and could suffer considerably for low signal-to-noise ratios (SNRs).

It is important to note that there are two sets of suboptimal estimates for ω_o, d, and φ_o corresponding to the two carrier frequencies, whereas only one suboptimal estimate for R_o. In step 2 of the IRNLS, we only need a single suboptimal estimate of ω_o for initialization. In the absence of any *a priori* information on the operating conditions, for example, the SNR at the two carriers, one can simply average the suboptimal estimates to obtain a single value as $\omega_{osubopt} = (\omega_{o1,subopt} + \omega_{o2,subopt})/2$. However, more sophisticated strategies, such as $\omega_{osubopt} = w_1 \omega_{o1,subopt} + w_2 \omega_{o2,subopt}$, $w_1 + w_2 = 1$ can be used if prior knowledge of the operating conditions is available. Likewise for d and φ_o. It is further noted that the suboptimal estimates for R_o and ρ_i are not required to launch the IRNLS, as these parameters are not involved in step 2 maximizations in the IRNLS.

B. Rotational MD

Consider the single blade returns of (15). Ignoring the noise for the time being, the Fourier transform of

(15), denoted as $X_i(\omega)$, is given by

$$X_i(\omega) = H_i(\omega;\boldsymbol{\psi}') * e^{j4\pi f_i R_o/c} \sum_{m=-\infty}^{\infty} j^m J_m(d) e^{-jm\varphi_o} \delta(\omega - m\omega_o) \tag{26}$$

where '$*$' denotes the convolution operator, and $H_i(\omega;\boldsymbol{\psi}')$ is the Fourier transform of $h_i(n;\boldsymbol{\psi}')$. The sinc fluctuation in $h_i(n;\boldsymbol{\psi}')$ can be expressed in terms of the spherical Bessel function of zero order, denoted by $j_o(\cdot)$, leading to [21]

$$h_i(n;\boldsymbol{\psi}') = \rho_i j_o\left(\frac{4\pi f_i d\cos(\omega_o n - \varphi_o)}{c}\right) \tag{27}$$

Expressing $j_o(\cdot)$ in terms of the Bessel function of the first kind, and using its integral equivalent, we obtain

$$\begin{aligned} h_i(n;\boldsymbol{\psi}') &= \rho_i \sqrt{\frac{\pi}{2\left(\frac{4\pi f_i d\cos(\omega_o n - \varphi_o)}{c}\right)}} J_{1/2}\left(\frac{4\pi f_i d\cos(\omega_o n - \varphi_o)}{c}\right) \\ &= \frac{\rho_i\sqrt{\pi}}{\Gamma(1)\Gamma(1/2)} \int_0^1 \cos\left(\frac{4\pi f_i d\cos(\omega_o n - \varphi_o)}{c} y\right) dy \end{aligned} \tag{28}$$

where $\Gamma(\cdot)$ denotes the gamma function. The integrand in (28) can be simplified further using the Jacobi-Anger series [21],

$$\cos\left(\frac{4\pi f_i d\cos(\omega_o n - \varphi_o)}{c} y\right) = J_o\left(\frac{4\pi f_i d}{c} y\right) + 2\sum_{m=1}^{\infty} (-1)^m J_{2m}\left(\frac{4\pi f_i d}{c} y\right) \cos(m(2\omega_o n - 2\varphi_o)) \tag{29}$$

Using (29) in (28), and then applying the Fourier transform, we obtain

$$H_i(\omega;\boldsymbol{\psi}') = \frac{2\pi\rho_i\sqrt{\pi}}{\Gamma(1)\Gamma(1/2)} \int_0^1 \left[\begin{array}{l} J_o\left(\frac{4\pi f_i d}{c} y\right)\delta(0) + \\ \sum_{m=1}^{\infty} (-1)^m J_{2m}\left(\frac{4\pi f_i d}{c} y\right)\left(\delta(\omega - 2m\omega_o)e^{-2mj\varphi_o} + \delta(\omega + 2m\omega_o)e^{2mj\varphi_o}\right) \end{array} \right] dy \tag{30}$$

Using the identity $\int_0^a J_v(x)dx = 2\sum_{r=1}^{\infty} J_{v+2r+1}(a)$, in (30), we obtain

$$H_i(\omega;\boldsymbol{\psi}') = \frac{\rho_i\sqrt{\pi}}{\Gamma(1)\Gamma(1/2)} \times \frac{c}{f_i d}\left[\begin{array}{l} \sum_{r=1}^{\infty} J_{0+2r+1}(\frac{4\pi f_i d}{c})\delta(0) \\ +\sum_{m=1}^{\infty}(-1)^m \left(\begin{array}{l}\delta(\omega-2m\omega_o)e^{-2mj\varphi_o} \\ +\delta(\omega+2m\omega_o)e^{2mj\varphi_o}\end{array}\right)\sum_{r=1}^{\infty} J_{2m+2r+1}(\frac{4\pi f_i d}{c}) \end{array}\right] \tag{31}$$

Interestingly, the function in (31) has harmonics at $0, \pm 2\omega_o, \pm 4\omega_o, \ldots,$ where amplitudes are scaled by a complex combination of Bessel functions. From (26) and using the result in (31), it can be readily seen that the resulting expression after convolution retains the original harmonic structure, i.e., the spectrum $X_i(\omega)$ has peaks at $0, \pm\omega_o, \pm 2\omega_o, \ldots \infty,$ akin to the vibrational MD spectrum. Likewise, it can be shown that, for Q identical blades, the Fourier spectrum of has harmonics at $0, \pm Q\omega_o, \pm 2Q\omega_o, \ldots \infty$. In practice, similar to the vibrational MD case, there exist only a finite number of dominant harmonics for rotational MD. In essence, the suboptimal estimator, designed for the vibrational MD, can be also used for rotational MD to estimate $Q\omega_o,$ from which the suboptimal estimate of the rotational frequency denoted as $\hat{\omega}_{oi,subopt}, i = 1,2$ is readily obtained.

Unlike the vibrational MD case, it is not straightforward to use the amplitude of the peaks in the return signal spectrum to obtain suboptimal estimates of d and φ_o for rotational MD. This is due to the complicated structure of (31) and (26) involving Bessel functions and convolution. Instead, we use the grid search technique for estimating d and φ_o. The suboptimal estimates for d and φ_o at each of the carrier frequencies are readily obtained as,

$$\begin{aligned} (\hat{d}_{i,subopt}, \hat{\varphi}_{oi,subopt}) &= \arg\max_{d,\varphi_o} \ \mathrm{G}_i(\hat{\omega}_{oi,subopt}, d, \varphi_o) \\ \mathrm{G}_i(\omega_o d, \varphi_o) &= \frac{\left|\sum_{n=0}^{N-1} x_i(n) e^{-j4\pi f_i d\cos(\omega_o n - \varphi_o)/c}\right|^2}{\sum_{n=0}^{N-1}\gamma_i^2(n;\boldsymbol{\psi})} \end{aligned} \tag{32}$$

The cost function $\mathrm{G}_i(\omega_o d, \varphi_o)$ is easily recognized as the ML cost function operating individually on the returns at the carrier f_i. Although (32) is designed for a single blade, it can be used directly when

multiple blades are present. In fact, the presence of Q blades will reveal itself as Q dominant peaks in the cost function (32), provided that Q is finite.

The grid search on (32) is appealing because of two main reasons. Firstly, as opposed to traditional targets, rotating fans do not assume very high displacements. Thus, we can safely assume $d \in (0,1m]$. Further, $\varphi_o \in [0,2\pi)$. The entire parameter space can then be evaluated using a small and finite grid. For example, we can evaluate (32) for every 0.01m in the d-domain, and similarly for every 0.01π in the φ_o-domain, which makes the grid search extremely feasible. Secondly, the visualization of the cost function using the grid search would indicate the global optimum corresponding to one blade, or several maxima corresponding to multiple blades in the radar returns. In other words, knowledge of the number of blades can be readily obtained, if it is not known *a priori*. For a reasonable SNR, the cost function in (32) will fail to reveal multiple peaks when $Q \to \infty$, which is quite unlikely for fans, or when the grid size is too large to accommodate the support of all the peaks in the (d, φ_o) plane, in which case a single continuous peak is seen along the φ_o-axis.

Note that the suboptimal techniques for vibrational and to some extent rotational MD use the discrete Fourier transform, and thus, can be implemented using the FFT efficiently. It is now assumed that these suboptimal techniques give rise to estimates close to the true parameters so that the IRNLS-ML iterations converge to the optimal ML estimate.

V. CRAMÉR-RAO BOUNDS

The vibrational MD CRBs were derived in [14]. In this section, we derive the multi-component rotational MD CRBs. Let $\mathbf{F}$ be the Fisher information matrix and $\boldsymbol{\theta} = [\boldsymbol{\psi}^T, \sigma_1^2, \sigma_2^2]^T$ be the complete parameter vector, where the MD parameter vector is defined as $\boldsymbol{\psi} = [R_o, \omega_o, d, \varphi_o, \rho_1, \rho_2]^T$. The FIM elements can be derived in a compact manner for the complex Gaussian pdf due to the Slepian-Bangs formula, which is given by [15],[25],

$$F_{\theta_r\theta_s} = Tr\left\{\mathbf{C}^{-1}\frac{\partial \mathbf{C}}{\partial \theta_r}\mathbf{C}^{-1}\frac{\partial \mathbf{C}}{\partial \theta_s}\right\} + 2\,\mathrm{Re}\left\{\frac{\partial \boldsymbol{\mu}}{\partial \theta_r}^{H}\mathbf{C}^{-1}\frac{\partial \boldsymbol{\mu}}{\partial \theta_s}\right\},\ (r,s)\in(1,2,\ldots,8) \tag{33}$$

where $\boldsymbol{\mu}$ and $\mathbf{C}$ are the mean and the covariance matrix of the PDF, respectively. For the problem at hand, and using (33), it can be readily shown that

$$\begin{aligned} F_{\psi_r\psi_s} &= 2\,\mathrm{Re}\left\{\mathbf{1}^T\mathbf{E}_{\psi_r}^H\mathbf{C}^{-1}\mathbf{E}_{\psi_s}\mathbf{1}\right\}, (r,s)\in(1,2,\ldots,6) \\ \mathbf{E}_{\psi_r} &= \begin{bmatrix}\mathbf{E}_{1,\psi_r}\\ \mathbf{E}_{2,\psi_r}\end{bmatrix}\in\Im^{2N\times Q},\ \mathbf{E}_{i,\psi_r} = \left[\mathbf{e}_{i1}^{\psi_r},\mathbf{e}_{i2}^{\psi_r},\ldots,\mathbf{e}_{iQ}^{\psi_r}\right] \\ \mathbf{e}_{iq}^{\psi_r} &:= \frac{\partial}{\partial \psi_r}\boldsymbol{\beta}_{iq}(\boldsymbol{\psi}) = \frac{\partial}{\partial \psi_r}\left(\rho_i e^{j4\pi f_i R_o/c}\times\boldsymbol{\gamma}_{iq}(\boldsymbol{\psi}')\odot\mathbf{g}_{iq}(\boldsymbol{\psi}')\right) \end{aligned} \tag{34}$$

where $\boldsymbol{\gamma}_{iq}(\boldsymbol{\psi}')$ and $\mathbf{g}_{iq}(\boldsymbol{\psi}')$ have been defined in (18). The derivatives with respect to the parameters are required. The partial derivatives of $\boldsymbol{\beta}_{iq}(\boldsymbol{\psi})$ with respect to $\psi_r, r=1,2,\ldots,6$ are given by,

$$\frac{\partial}{\partial R_o}\boldsymbol{\beta}_{iq}(\boldsymbol{\psi}) = \frac{j4\pi f_i}{c}\boldsymbol{\beta}_{iq}(\boldsymbol{\psi}),\ \frac{\partial}{\partial \rho_i}\boldsymbol{\beta}_{iq}(\boldsymbol{\psi}) = \rho_i^{-1}\boldsymbol{\beta}_{iq}(\boldsymbol{\psi}) \tag{35}$$

$$\begin{aligned} \frac{\partial}{\partial \omega_o}\boldsymbol{\beta}_{iq}(\boldsymbol{\psi}) &= \rho_i e^{j4\pi f_i R_o/c}\left(\frac{\partial \boldsymbol{\gamma}_{iq}(\boldsymbol{\psi}')}{\partial \omega_o}\odot\mathbf{g}_{iq}(\boldsymbol{\psi}') + \boldsymbol{\gamma}_{iq}(\boldsymbol{\psi}')\odot\mathbf{g}_{iq}(\boldsymbol{\psi}')\odot\mathbf{n}\odot\mathrm{Im}\{\boldsymbol{\xi}_q\}\times\frac{-j4\pi f_i d}{c}\right) \\ \boldsymbol{\xi}_q &:= [1, e^{j\omega_o}, e^{2j\omega_o},\ldots,e^{j(N-1)\omega_o}]^T\times e^{-j\varphi_q},\ \mathbf{n} := [0,1,2\ldots,N-1]^T \\ \frac{\partial \boldsymbol{\gamma}_{iq}(\boldsymbol{\psi}')}{\partial \omega_o} &:= \begin{pmatrix}\mathrm{Re}\{\mathbf{g}_{iq}(\boldsymbol{\psi}')\}\odot\frac{-4\pi f_i d}{c}\mathbf{n}\odot\mathrm{Im}\{\boldsymbol{\xi}_q\}\odot\frac{4\pi f_i d}{c}\mathrm{Re}\{\boldsymbol{\xi}_q\}\\ -\mathrm{Im}\{\mathbf{g}_{iq}(\boldsymbol{\psi}')\}\odot\frac{-4\pi f_i d}{c}\mathbf{n}\odot\mathrm{Im}\{\boldsymbol{\xi}_q\}\end{pmatrix}\odot(\mathbf{v}^{\odot-2}) \\ \mathbf{v} &:= \frac{4\pi f_i d}{c}\mathrm{Re}\{\boldsymbol{\xi}_q\} \end{aligned} \tag{36}$$

where we define $(\cdot)^{\odot-k}$ as the element-wise division of a vector or a matrix raised to *k*-th power, i.e., if $\mathbf{x}=[x_1,x_2,\ldots,x_N]^T, \mathbf{x}^{\odot-k}=[1/x_1^k,1/x_2^k,\ldots,1/x_N^k]^T$. Using the same convention, the other derivatives which are required for evaluating the FIM are provided below.

$$\frac{\partial}{\partial d}\boldsymbol{\beta}_{iq}(\boldsymbol{\psi}) = \rho_i e^{j4\pi f_i R_o/c}\left(\frac{\partial \boldsymbol{\gamma}_{iq}(\boldsymbol{\psi}')}{\partial d}\odot \mathbf{g}_{iq}(\boldsymbol{\psi}') + \boldsymbol{\gamma}_{iq}(\boldsymbol{\psi}')\odot \mathbf{g}_{iq}(\boldsymbol{\psi}')\odot \mathrm{Re}\{\boldsymbol{\xi}_q\}\times\frac{j4\pi f_i}{c}\right)$$

$$\frac{\partial \boldsymbol{\gamma}_{iq}(\boldsymbol{\psi}')}{\partial d} := \begin{pmatrix} \mathrm{Re}\{\mathbf{g}_{iq}(\boldsymbol{\psi}')\}\odot\frac{4\pi f_i}{c}\mathrm{Re}\{\boldsymbol{\xi}_q\}\odot\frac{4\pi f_i d}{c}\mathrm{Re}\{\boldsymbol{\xi}_q\} \\ -\mathrm{Im}\{\mathbf{g}_{iq}(\boldsymbol{\psi}')\}\odot\frac{4\pi f_i}{c}\mathrm{Re}\{\boldsymbol{\xi}_q\}\end{pmatrix}\odot(\mathbf{v}^{\odot -2}) \tag{37}$$

$$\frac{\partial}{\partial \varphi_o}\boldsymbol{\beta}_{iq}(\boldsymbol{\psi}) = \rho_i e^{j4\pi f_i R_o/c}\left(\frac{\partial \boldsymbol{\gamma}_{iq}(\boldsymbol{\psi}')}{\partial \varphi_o}\odot \mathbf{g}_{iq}(\boldsymbol{\psi}') + \boldsymbol{\gamma}_{iq}(\boldsymbol{\psi}')\odot \mathbf{g}_{iq}(\boldsymbol{\psi}')\odot \mathrm{Im}\{\boldsymbol{\xi}_q\}\times\frac{j4\pi f_i d}{c}\right)$$

$$\frac{\partial \boldsymbol{\gamma}_{iq}(\boldsymbol{\psi}')}{\partial \varphi_o} := \begin{pmatrix} \mathrm{Re}\{\mathbf{g}_{iq}(\boldsymbol{\psi}')\}\odot\frac{4\pi f_i d}{c}\mathrm{Im}\{\boldsymbol{\xi}_q\}\odot\frac{4\pi f_i d}{c}\mathrm{Re}\{\boldsymbol{\xi}_q\} \\ -\mathrm{Im}\{\mathbf{g}_{iq}(\boldsymbol{\psi}')\}\odot\frac{4\pi f_i d}{c}\mathrm{Im}\{\boldsymbol{\xi}_q\}\end{pmatrix}\odot(\mathbf{v}^{\odot -2}) \tag{38}$$

From (33), two important observations are in order. First, the cross FIM elements with respect to ρ_i and the parameter R_o are zero for a single fan blade, and are in general non-zero when multiple blades are present, i.e,

$$F_{\rho_i R_o} = 0,\ i = 1,\ 2,\ Q = 1 \tag{39}$$

This is because the amplitude, ρ_i, $i = 1,2$ is not embedded in the phase of the signal, and similarly the range parameter R_o is not a function of $h_i(n;\boldsymbol{\psi}')$. The more important second observation arises from the fact that since the covariance matrix is not a function of the parameters in $\boldsymbol{\psi}$, the cross FIM elements with respect to σ_i^2 and all the parameters in $\boldsymbol{\psi}$ are zero, i.e.,

$$F_{\sigma_i^2 \psi_r} = 0,\ r \in (1,\ldots,6),\ i = 1,2,\ \forall Q \tag{40}$$

Eq. (40) implies that, regardless of the knowledge (or no knowledge) of the parameters, σ_i^2, the CRBs depend only on the inverted FIM of the MD parameters, including the range. Further simplifications of the FIM elements are tedious to derive. The above equations can be used to numerically evaluate the FIM and the CRBs.

VI. SIMULATION AND EXPERIMENTAL RESULTS

A. Simulations

The carrier frequencies for the dual frequency operation are set to $f_1 = 903\,\text{MHz}$ and $f_2 = 921\,\text{MHz}$. Also, we average the suboptimal estimates of parameters, such as ω_o, d, and φ_o, corresponding to the two carrier frequencies, and use the averaged values for IRNLS initialization.

We first consider the vibrational MD. For simplicity we assume $\rho_i = \rho$. The SNRs for this case are defined as $SNR_i = \|\mathbf{s}_i\|^2 / \sigma_i^2 N, \forall i = 1,2$. We force $SNR_1 = 10\,\text{dB}$ and vary SNR_2 from -10dB onwards, in increments of 5 dB. Figures 2(a)-(d) demonstrate the MSE for the IRNLS and the suboptimal estimation schemes. The number of Monte Carlo trials was 250 and the maximum number of allowed iterations, $k_{\max}$, was chosen as 10. The number of data samples $N = 1024$, and the parameters of the MD signal used were $\boldsymbol{\psi} = [R_o = 1.3m, d = 0.07m, \omega_o = 0.123\pi, \varphi_o = \pi/3]^T$. The received signal is wideband for the aforementioned carrier frequencies. In the suboptimal estimation scheme, we forced $m = K = 1$ which makes $\mathbf{K} = [-1,0,1]^T$ in eqs. (21), (23), and (25). This choice of K provides satisfactory results, and amounts to using the first harmonic and DC for estimation, i.e., the suboptimal scheme operates in a narrowband framework. The estimates after the first iteration of the IRNLS correspond to optimizing the NLS cost function $\sum_{i=1}^{2} \|\mathbf{x}_i - \mathbf{s}_i(\boldsymbol{\psi})\|^2 / N$, and are also provided in Fig. 2 for comparison. It is clear from Fig. 2(a)-(d) that the IRNLS gives better MSE than the NLS and of course the suboptimal schemes. The corresponding CRBs for single frequency and dual frequency operations are also shown. It is clear that the single frequency CRBs guide the ML behavior for the dual frequency operations. The estimates are clearly above the dual-frequency CRBs. The IRNLS offers superior performance than the NLS for all parameters except R_o for which both the NLS and IRNLS give similar MSE. It is noted that when

$SNR_1 = SNR_2 \Rightarrow \sigma_1^2 = \sigma_2^2$, the IRNLS and NLS MSE are the same for all parameters. It is clear that the MSE of the parameters decreases with the SNR, specifically SNR_2 as predicted by the CRBs.

Next, we consider a rotating fan with multiple blades. Figs. 3 and 4 shows the corresponding CRBs with respect to SNR_2 and the data record length, N, respectively. The parameters used in generating these figures were $\boldsymbol{\psi} = [R_o = 1.4m, d = 0.253m, \omega_o = 0.02\pi, \varphi_o = \pi/8]^T$. The number of blades vary from one to four. From Fig. 3, it is evident that multiple blades yield better estimates for all the parameters. However, from Fig. 4, we observe that,for a fixed SNR and varying *N*, the CRBs corresponding to multiple blades are more or less similar to those for a single. In general, for the case of multiple identical blades, greater confidence in the estimates can be obtained which implies better estimation of the parameters. Consider, for example, the time-frequency distribution of a four blade return. The instantaneous frequency (IF) for the blades is identical in structure but differs in the phase parameter φ_p. It is clear that, for example, the rotational frequency can be estimated with a greater confidence since four different IF curves in the TF plane can be used jointly to estimate the rotational frequency, rather than a single IF curve when a single blade is present, provided that the IF curves are mostly non-overlapping in the TF plane. The performance of the NLS and IRNLS and suboptimal estimators for the rotational MD corresponding to a fan with three blades is shown in Fig. 5. Parameters identical to those for Figs. 3 and 4 were used in Fig. 5. For generating the MSE, the number of Monte Carlo trials was set to 200, and the maximum number of allowed iterations, $k_{\max}$, was chosen as 10. A coarse grid search was used as in (32) to suboptimally estimate the parameters d and φ_o. In the rotational MD simulations, we used the root-MUSIC algorithm to estimate the harmonics instead of peak picking in order to compute the MSE for SNR values less than 0dB. In Fig. 6(a), we show the LLcost as given in (8a), as well as the norm of the difference in parameter estimates for various iterations in the IRNLS in Fig. 6(b). Parameters identical to the rotational MD simulation of Fig. 5 were used to generate Fig. 6, except that we show one Monte Carlo simulation, and $(SNR_1, SNR_2) = (10, 5)$ dB. It is clear from Fig. 6(b) that after six iterations of the IRNLS, the norm

becomes zero. In essence, there exists a cluster or accumulation point as shown in Fig. (6b). The discussion in Appendix-A gives more details on the cluster point with respect to the IRNLS.

B. *Experimental Results*

In this section, we present results of IRNLS applied to various MD signal returns measured using a dual-frequency radar in a laboratory setting. First, a 12in conducting sphere was tied to the ceiling with a nylon string, and excited to oscillate in a simple harmonic fashion. This experiment corresponds to the vibrational MD scenario. The approximate range to the target was 16.4ft or 4.99m, the carrier frequencies were chosen to be 906.3 and 919.6 MHz, and the sampling frequency was 100Hz. More details on the experiment can be found in [26]. We processed only the first seven seconds of data, comprising 700 samples, in order to avoid damped oscillations. Figure 7 shows the IRNLS, NLS, and suboptimal instantaneous frequency (IF) trajectories overlaid on the spectrogram of the data. Clearly, the IRNLS yields better estimates when compared to the NLS, and agrees with the IF of the data for both carrier frequencies. The range estimates for IRNLS and NLS were 4.89m and 4.83m, respectively.

Second, the IRNLS is applied to measured returns from a table-top fan with 4-metallic blades. The carrier frequencies are chosen as 903.6 MHz and 921 MHz. The distance from the center of the fan to the radar was 3 m, and the sampling frequency was chosen to be 5 kHz to avoid aliasing. Two datasets, one for azimuth equal to 0°, and the other for 60° azimuth, were used for the ML analysis. Fig. 8(a) shows the spectrogram of the raw data for 0° azimuthal aspect, using a rectangular window of 101 samples which corresponds to around 130 % of the period of the rotation. For subsequent ML analysis, the data was decimated by a factor of 5. The 2D grid search cost function, as given in (32) was used, and the cost function is shown in Fig. 8(b) for the second carrier. The grid was initialized with the rotational frequency estimate obtained from the Fourier spectrum. We can clearly see 4 dominant peaks corresponding to the 4 blades. The suboptimal estimates were used to initialize the ML algorithm. The range estimates and final LL costs are provided in Table I. The results in Table I indicate that both the NLS and IRNLS perform exceptionally well for this dataset. Fig. 9(a) shows the spectrogram of the raw data (not resampled),

corresponding to 60^o azimuthal aspect, using the same window length as in Fig. 8(a). The 2D grid search cost function corresponding to the second carrier frequency is shown in Fig. 9(b). Similar to Fig. 8(b), the 2D grid in Fig. 9(b) clearly shows 4 dominant peaks. The corresponding ML estimates for the range are shown in Table II, which shows that the IRNLS performs better than the NLS.

VII. CONCLUSIONS

In this paper, we considered dual frequency Doppler radars for range estimation of moving targets with application to urban sensing. The ML estimator was derived for the micro-Doppler motion profile, which is commonly exhibited by indoor moving targets. It was shown that the ML estimator, although not solvable in closed form, can be provided using a step-wise iterative algorithm termed as the IRNLS. The algorithms solution and procedure depends on the motion profile model. The initial conditions are provided using suboptimal values which rely on the harmonic nature of the radar returns. For simulated data, the algorithm was shown to be superior in terms of the MSE when compared to suboptimal estimators. The iterative ML was also applied to data measurements corresponding to indoor moving targets, yielding superior IF estimates and good estimates of the range.

Appendix

Convergence of IRNLS

In this appendix, we do not assume any specific motion profile. The results are general and applicable to $\boldsymbol{\theta} = [\boldsymbol{\psi}^T, \sigma_1^2, \sigma_2^2]^T, \boldsymbol{\psi} = [\psi_1, \psi_2, \psi_3 ..... \psi_p]^T$ for the IRNLS.

Proposition 1: The FIM for the dual frequency radar can be expressed as

$$\mathbf{F}(\boldsymbol{\theta}) = \begin{bmatrix} \mathbf{F}(\boldsymbol{\psi}) & 0 & 0 \\ 0 & N/\sigma_1^4 & 0 \\ 0 & 0 & N/\sigma_2^4 \end{bmatrix} \tag{A.1}$$

Proof: The proof of the above proposition is standard and can be easily obtained using the Slepian-Bangs formula [15],[25].

Proposition 2: If the minimization in (10) is carried out using the method of Fisher scoring, with step size equal to unity, then the IRNLS algorithm becomes the Fisher scoring technique for the ML problem.

Proof: We first note that for a fixed arbitrary covariance matrix, the gradient vector with respect to the desired parameter vector $\boldsymbol{\psi}$ of the negative LL is identical to the gradient vector of the cost function in (10). Hence, the Fisher scoring technique for the k^{th} iteration for estimating $\boldsymbol{\psi}_k$ is then given as [27]

$$\hat{\boldsymbol{\psi}}_k = \hat{\boldsymbol{\psi}}_{k-1} - \lambda_k \mathbf{F}^{-1}(\hat{\boldsymbol{\psi}}_{k-1})(-\nabla \mathbf{J}(\hat{\boldsymbol{\psi}}_{k-1})) \tag{A.2}$$

where $\mathbf{F}^{-1}(\hat{\boldsymbol{\psi}}_{k-1})$ and $-\nabla \mathbf{J}(\hat{\boldsymbol{\psi}}_{k-1})$ are the FIM, and the gradient vector of the cost function in (10), obtained using the previous estimate, and λ_k is the step size parameter. The negative sign in (A.2) preceding the second term indicates the minimization of the cost function (10), or equivalently minimization of the negative LL[2]. The Fisher scoring applied to the negative LL for the entire parameter vector $\boldsymbol{\theta}$, takes the following form.

$$\hat{\boldsymbol{\theta}}_k = \hat{\boldsymbol{\theta}}_{k-1} - \lambda_k \begin{bmatrix} \mathbf{F}^{-1}(\hat{\boldsymbol{\psi}}_{k-1}) & 0 & 0 \\ 0 & \hat{\sigma}^4_{1(k-1)} / N & 0 \\ 0 & 0 & \hat{\sigma}^4_{2(k-1)} / N \end{bmatrix} \begin{bmatrix} -\nabla \mathbf{J}(\boldsymbol{\psi}) \\ -\partial \ln(p(\mathbf{x};\boldsymbol{\psi}) / \partial \sigma_1^2 \\ -\partial \ln(p(\mathbf{x};\boldsymbol{\psi}) / \partial \sigma_2^2 \end{bmatrix}_{\boldsymbol{\psi}=\hat{\boldsymbol{\psi}}_{k-1}, \sigma_i^2=\sigma^2_{i(k-1)}, i=1,2} \tag{A.3}$$

The term $-\partial \ln(p(\mathbf{x};\boldsymbol{\psi})) / \partial \sigma_i^2,\ \forall i = 1,2$ was an intermediate step in deriving (7). Using this intermediate step with $\lambda_k = 1,$ and multiplying the matrix and the gradient vector in (A.3), we obtain (A.2) with $\lambda_k = 1,$ and

$$\hat{\sigma}^2_{ik} = \left\| \mathbf{x}_i - \mathbf{s}_i(\hat{\boldsymbol{\psi}}_{k-1}) \right\|^2 / N,\ \forall i = 1,2 \tag{A.4}$$

Equation (A.4) is the remaining key equation in the IRNLS for updating in (10). Q. E. D.

The special case of $\lambda_k = 1$ is oftentimes used in the literature (see [15], and also [27]).The above proposition implies that the IRNLS is a special case of Fisher scoring algorithm. However, as well known, the Fisher scoring converges if the suboptimal estimates used to initialize it are close to the optimal ML solution. In [27, remark 4.1 and remark 4.2], under certain conditions it was shown that the Fisher scoring

[2] The sign is flipped for the conventional Fisher scoring technique which is applied to the maximizing the LL [27].

method converges to at least a local minimum of the negative LL as $N \to \infty$, i.e., asymptotically. The same follows from proposition 2 for the IRNLS, more details can be seen in [27]. If the negative LL objective is convex, which is a standard assumption for ML techniques, then the Fisher scoring converges surely to the global minimum [28]. Convergence is also attained if the initialization is contained within a set including the optimal solution, where the objective is locally convex [28]. For step-wise iterative ML schemes, an interesting result is provided in [29, lemma-1], where the authors prove the existence of a cluster point or an accumulation point, denoted as $\boldsymbol{\theta}'$, for the sequence of parameter iterates given by $\{\boldsymbol{\theta}_k\}$ if the negative LL is bounded below, which is definitely satisfied by the Gaussian pdf. We can, thus, deduce that the IRNLS iterates also exhibit similar behavior. Essentially, if there exists a unique cluster point $\boldsymbol{\theta}'$ for any sequence $\{\boldsymbol{\theta}_k\}$, then $\boldsymbol{\theta}'$ is the ML solution $\hat{\boldsymbol{\theta}}(\mathbf{x})$. This directly implies that $\lim_{k\to\infty} \|\boldsymbol{\theta}_{k+1} - \boldsymbol{\theta}_k\| = 0$. The existence of the cluster point was also proven in [28] for the constrained Fisher scoring technique. We now prove that the Fisher scoring and hence the IRNLS increases the LL for every iteration monotonically.

Proposition 3: Under certain assumptions, the Fisher scoring and hence the IRNLS increases the LL for every k, until convergence as $N \to \infty$.

Proof: It is required to prove $\ln(p(\mathbf{x};\boldsymbol{\theta}_{k+1})) - \ln(p(\mathbf{x};\boldsymbol{\theta}_k)) > 0$. Expanding the pdf about the arbitrary point $\lambda_k \mathbf{F}^{-1}(\boldsymbol{\theta}_k)\nabla\mathbf{J}(\boldsymbol{\theta}_k)$, where $\nabla\mathbf{J}(\boldsymbol{\theta}_k)$ is the gradient of the LL evaluated at the previous $\boldsymbol{\theta}_k$, using the Taylor series expansion.

$$\begin{aligned} \ln(\mathbf{x};\boldsymbol{\theta}_{k+1}) - \ln(\mathbf{x};\boldsymbol{\theta}_k) &= \lambda_k \nabla^T \mathbf{J}(\boldsymbol{\theta}_k)\mathbf{F}^{-1}(\boldsymbol{\theta}_k)\nabla\mathbf{J}(\boldsymbol{\theta}_k) \\ + \frac{\lambda_k^2}{2}\nabla^T \mathbf{J}(\boldsymbol{\theta}_k)(\mathbf{F}^T(\boldsymbol{\theta}_k))^{-1}[\nabla(\nabla^T \mathbf{J}(\boldsymbol{\theta}_k))]\nabla\mathbf{J}(\boldsymbol{\theta}_k)\mathbf{F}^{-1}(\boldsymbol{\theta}_k) & \\ + O\left(\left\|\mathbf{F}^{-1}(\boldsymbol{\theta}_k)\nabla\mathbf{J}(\boldsymbol{\theta}_k)\right\|\right) & \end{aligned} \tag{A.5}$$

where $[\nabla(\nabla^T \mathbf{J}(\boldsymbol{\theta}_k))]$ is the Hessian matrix evaluated at $\boldsymbol{\theta}_k$. Now using the results in [30], i.e., as $N \to \infty$ the negative Hessian matrix converges to the FIM with probability 1, we can replace the negative

Hessian matrix with the FIM, $\mathbf{F}(\boldsymbol{\theta}_k)$ in (A.5), further assuming that the LL can be approximated as a quadratic, i.e., ignoring the higher order terms, we get

$$\begin{aligned}\ln(\mathbf{x};\boldsymbol{\theta}_{k+1}) - \ln(\mathbf{x};\boldsymbol{\theta}_k) &= \lambda_k \nabla^T \mathbf{J}(\boldsymbol{\theta}_k)\mathbf{F}^{-1}(\boldsymbol{\theta}_k)\nabla \mathbf{J}(\boldsymbol{\theta}_k) - \frac{\lambda_k^2}{2}\nabla^T \mathbf{J}(\boldsymbol{\theta}_k)\mathbf{F}^{-1}(\boldsymbol{\theta}_k)\nabla \mathbf{J}(\boldsymbol{\theta}_k) \\ &= (\lambda_k - \lambda_k^2/2)\nabla^T \mathbf{J}(\boldsymbol{\theta}_k)\mathbf{F}^{-1}(\boldsymbol{\theta}_k)\nabla \mathbf{J}(\boldsymbol{\theta}_k)\end{aligned} \tag{A.6}$$

Since the FIM is nonsingular and positive definite $\forall \boldsymbol{\theta}_k$, with $\lambda_k \in (0,1]$, we have (A.6) is always positive, and becomes zero at the local optimum solution. This proves the proposition for the Fisher scoring approach. Likewise, substituting $\lambda_k = 1, \forall k$ it is readily seen that (A.6) is always positive. This proves the proposition for the IRNLS. Q. E.D.

In this Appendix, we have proved that the IRNLS is a special case of Fisher scoring. Therefore, some of the results for Fisher scoring directly follow through to the IRNLS. In the simulations, we demonstrate the existence of the cluster point and the monotonic increase in the LL objective for every iteration.

ACKNOWLEDGMENT

This work was supported in part by ONR under contract N00014-07-1-0043 and in part by DARPA under contract HR011-07-1-0001.

REFERENCES

[1] Journal of the Franklin Institute, Special Issue on 'Advances in Indoor Radar Imaging,' Sept. 2008, 345, (6)

[2] Proceedings of the 2008 IEEE International Conference on Acoustics, Speech, and Signal Processing, Special Session on 'Through-the-Wall Radar Imaging,' Las vegas, USA, Apr. 2008, pp. 5173-5196

[3] Borek, S. E.: 'An overview of through the wall surveillance for homeland security', Proc. 34th Applied Imagery and Pattern Recognition Workshop, Washington D.C., USA, Oct. 2005

[4] Proceedings of the 2005 IEEE AP-S International Symposium, Special Session on 'Through-Wall

Imaging and Sensing', Washington D.C., USA, Jul. 2005, 3B, pp. 317-341

[5] Skolnik , M. I.: 'Introduction to Radar Systems' (McGraw-Hill, New York, 3rd edn. 2002)

[6] Amin, M., Zemany, P. D., Setlur, P., and Ahmad, F.: 'Moving target localization for indoor imaging using dual frequency CW radars', Proc. IEEE Workshop on Sensor Array and Multi-channel Processing, Waltham, Massachusetts, USA, Jul. 12-14, 2006, pp. 367-371

[7] Ridenour, L. N.: 'Radar System Engineering', Vol. 1 of MIT Radiation Labaratory Series (McGraw-Hill, NY, 1947)

[8] Boyer, W. D.: 'A diplex, Doppler, phase comparison radar', IEEE Trans. Aerosp. Navig. Electron., 1963, ANE-10, (3), pp. 27-33

[9] Chen, V. C., Li, F., Ho, S. –S., and Wechsler, H.: 'Analysis of micro-Doppler signatures', IEE Proceedings Radar, Sonar and Navigation, Aug. 2003, (4), 150, pp. 271-276

[10] Thayaparan, T., Abrol., S, Riseborough, E., Stankovic, L., Lamothe, D., and Duff, G.: 'Analysis of radar micro-Doppler signatures from experimental helicopter and human data', IET Radar Sonar and Navig., Aug. 2007, 1, (4), pp. 289-299

[11] Smith, G., Woodbridge, K., Baker, C. J., and Griffiths, H.: 'Multistatic micro-Doppler radar signatures of personnel targets', IET Signal Processing, Special Issue on Time-Frequency Approach to Radar Detection, Imaging, and Classification, In press.

[12] Rife, D., and Boorstyn, R.: 'Single tone parameter estimation from discrete-time observations', IEEE Trans. Inf. Theory, Sept. 1974, 20, (5), pp. 581-598

[13] Saha, S., and Kay, S. M.: 'Maximum likelihood parameter estimation of superimposed chirps using Monte Carlo importance sampling', IEEE Trans. Sig. Proc., Feb. 2002, 50, (2), pp. 224-230

[14] Setlur, P., Amin, M., and Ahmad, F.: 'Dual frequency Doppler radar for indoor range estimation: Cramér-Rao bound analysis', IET Signal Processing, Special Issue on Time-Frequency Approach to Radar Detection, Imaging, and Classification, In press.

[15] Kay, S. M.: 'Fundamentals of Statistical Signal Processing, Volume: I, Estimation Theory' (Prentice Hall, Englewood Cliffs, NJ, 1993)

[16] Green, P. J.: 'Iteratively reweighted least squares for maximum likelihood estimation, and some robust and resistant alternatives', Journal of the Royal statistical society, 1984, 46, (2), pp. 149-192

[17] Huber, P. J.: 'Robust Statistics' (John Wiley, New York, 1981)

[18] Chen, V. C, and Ling, H.: 'Time-Frequency Transforms for Radar Imaging and Signal Analysis' (Artech House, Boston, 2002)

[19] Martin, J., and Mulgrew, B.: 'Analysis of the theoretical radar return signal from aircraft propeller blades', Proc. IEEE Radar Conf., Arlington, VA, USA, May 7-10, 1990, pp. 569-572

[20] Schneider, H.: 'Application of an autoregressive reflection model for the signal analysis of radar echoes from rotating objects," Proc. Int. Conf. Acoust., Speech, Signal Process., New York, NY, Apr. 11-14, 1988, pp. 1236-1239

[21] Abromowitz, M. and Stegun, I. A.: 'Handbook of Mathematical Functions with Formulas, Graphs, and Mathematical tables' (Dover Publications, New York, 1972)

[22] Gini, F., and Giannakis, G. B.: 'Hybrid FM-polynomial phase signal modeling: parameter estimation and Cramér-Rao bounds', IEEE Trans. Signal Process., Feb. 1999, 47, (2), pp. 363-377

[23] Huang, S.-R, Lerner, R. M., and Parker, K. J.: 'On estimating the amplitude of harmonic vibration from the Doppler spectrum of reflected signals', Journal Acou. Soc. of Amer., Dec. 1990, 88, (6), pp. 2702-2712

[24] Zhou, G., and Giannakis, G. B.: 'Parameter estimation of FM signals using cyclic statistics', Proc. IEEE Int. Symp.Time-Freq. Time-Scale Analysis., Philadelphia, PA, Oct. 25-28, 1994, pp. 248-251

[25] Stoica, P., and Moses, R.: 'Introduction to Spectral Analysis' (Prentice-Hall, New Jersey, 1997)

[26] Setlur, P., Amin, M., Ahmad, F., and Zemany, P. D.: 'Experiments on through-the-wall detection and ranging', Proc. SPIE Symposium on Defense and Security, Orlando, FL., Apr. 2007

[27] Osbourne, M. R.: 'Fisher's method of scoring', International Statistical Review, Apr. 1992, 60, (1), pp. 99-117

[28] Moore, T. J., Sadler, B. M., and Kozick, R. J.: 'Maximum-likelihood estimation, the Cramér-Rao bound, and the method of scoring with parameter constraints', IEEE Trans. Signal Process., Mar. 2008, 56, (3), pp. 895-907

[29] Oberhoefer, W., and Kmenta, J.: 'A general procedure for obtaining the maximum likelihood estimates in generalized regression methods', Econometrica, May 1974, 42, (3), pp. 579-590

[30] Serfling, R. J.: 'Approximation Theorems of Mathematical Statistics' (John Wiley, New York, 1980)

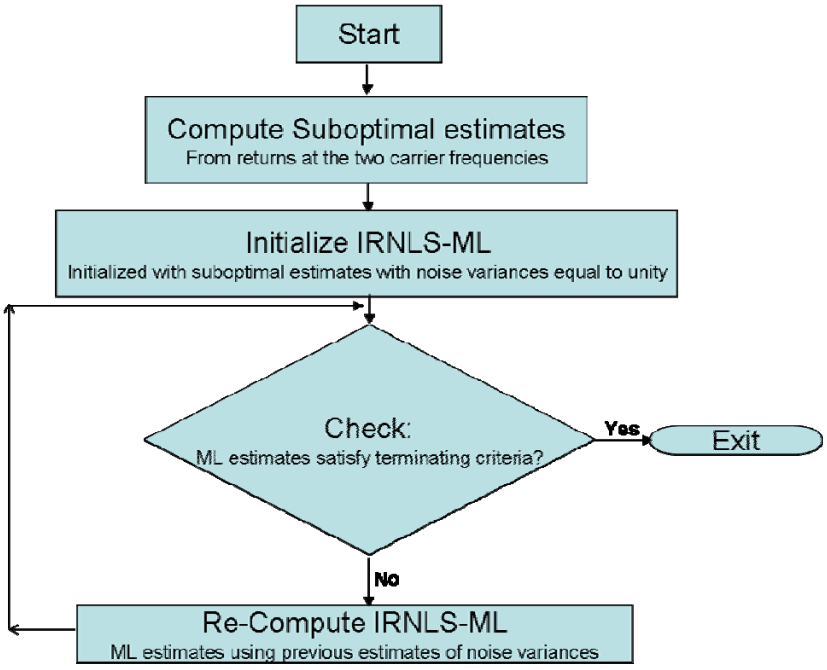

Fig. 1. Flowchart of IRNLS ML algorithm

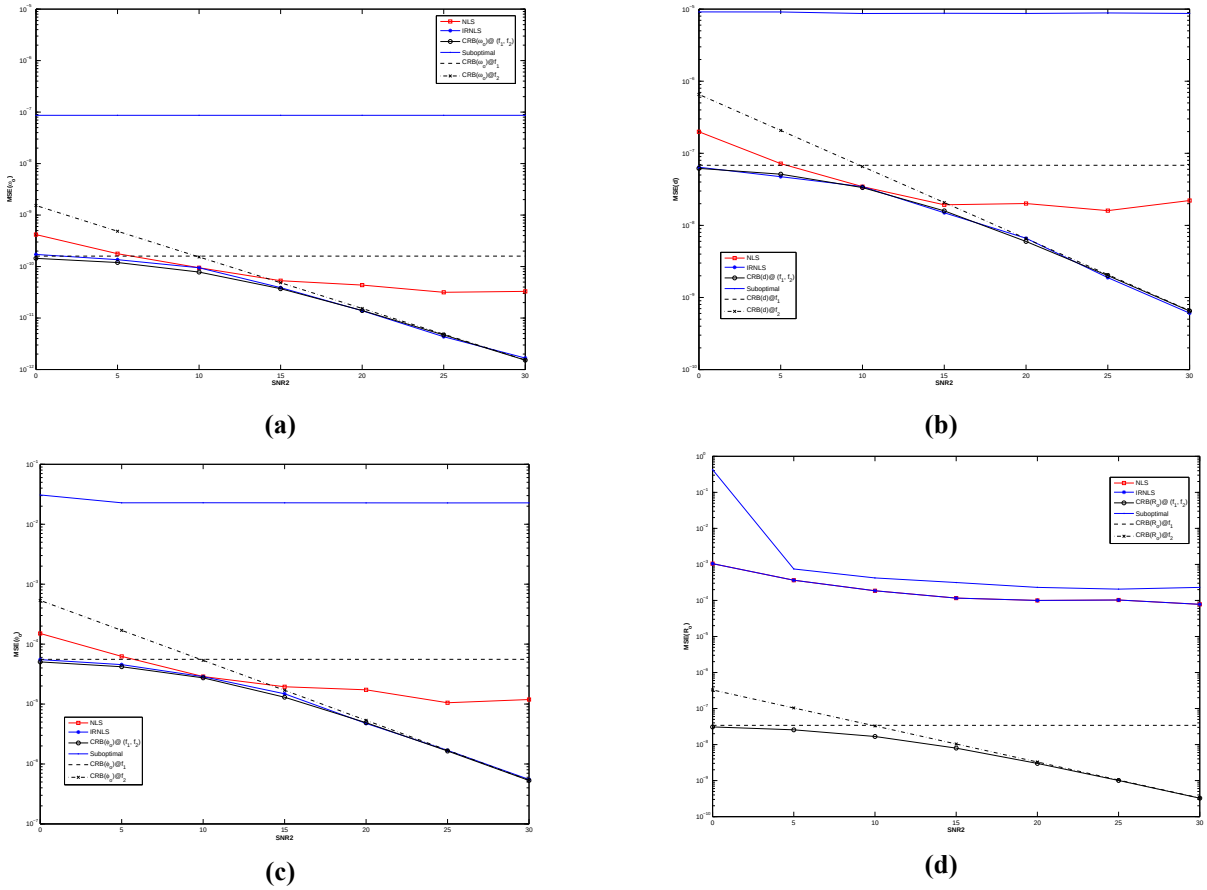

Fig. 2. MSE of vibrational MD parameters. IRNLS Comparsion wrt CRBs and NLS.

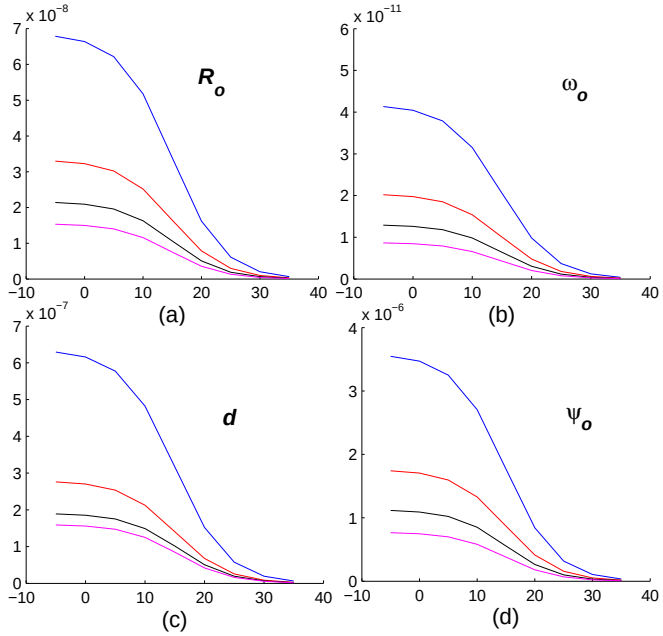

Fig.3 CRBs for multiple blades, N=512, SNR_1=15dB, x-axis SNR_2 dBs, y-axis CRBs, blue (1blade), red (2 blades), black (3 blades), magenta (4 blades).

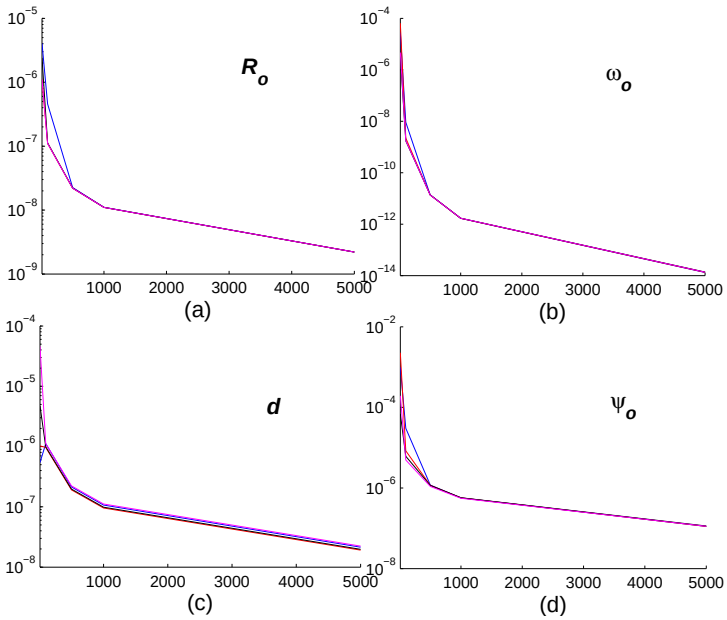

Fig.4 CRBs for multiple blades, SNR_1=15dB, SNR_2 =-10dB, x-axis *N*, data record length, y-axis CRBs, blue (1blade), red (2 blades), black (3 blades), magenta (4 blades).

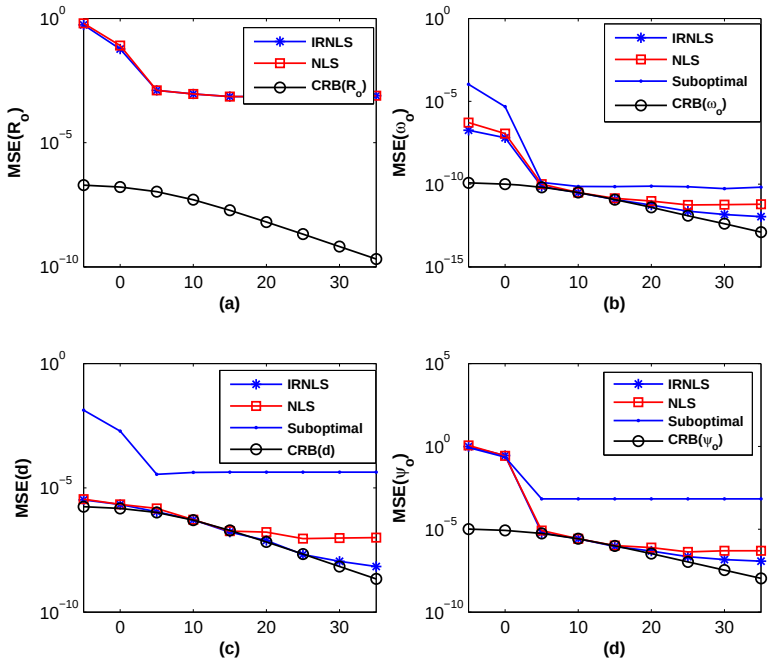

Fig. 5. MSE performance of rotational MD parameters, SNR_1=5dB, SNR_2 is varied.

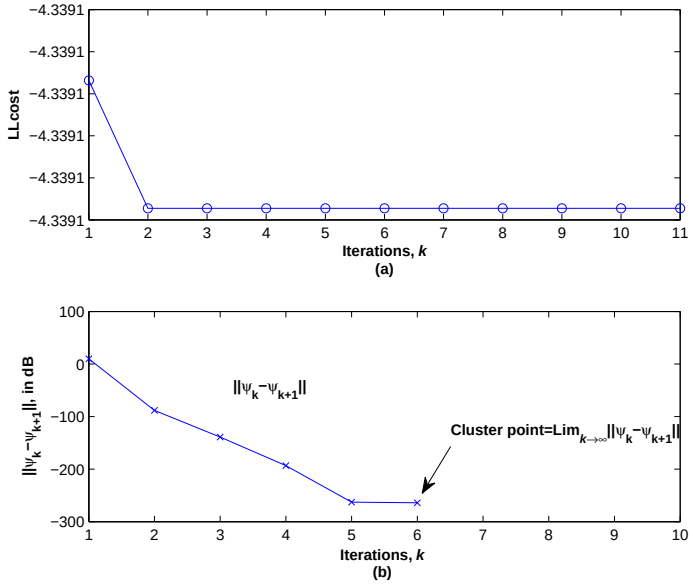

Fig. 6. Figures showing the (a) LL cost, (b) cluster point.

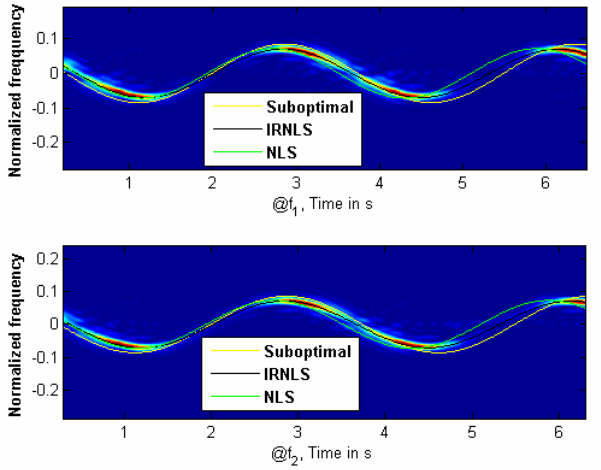

Fig. 7. Spectrogram of measured radar returns for vibrational MD, along with the final IF fits.

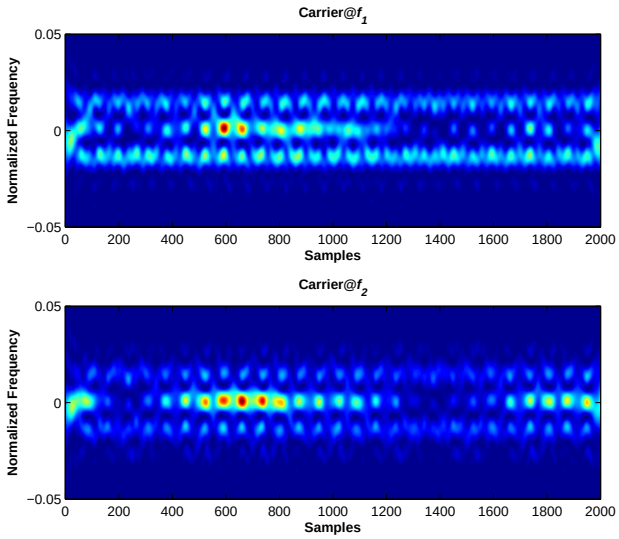

Fig. 8(a). Spectrograms of the measured returns at 0^o azimuth at the two carriers.

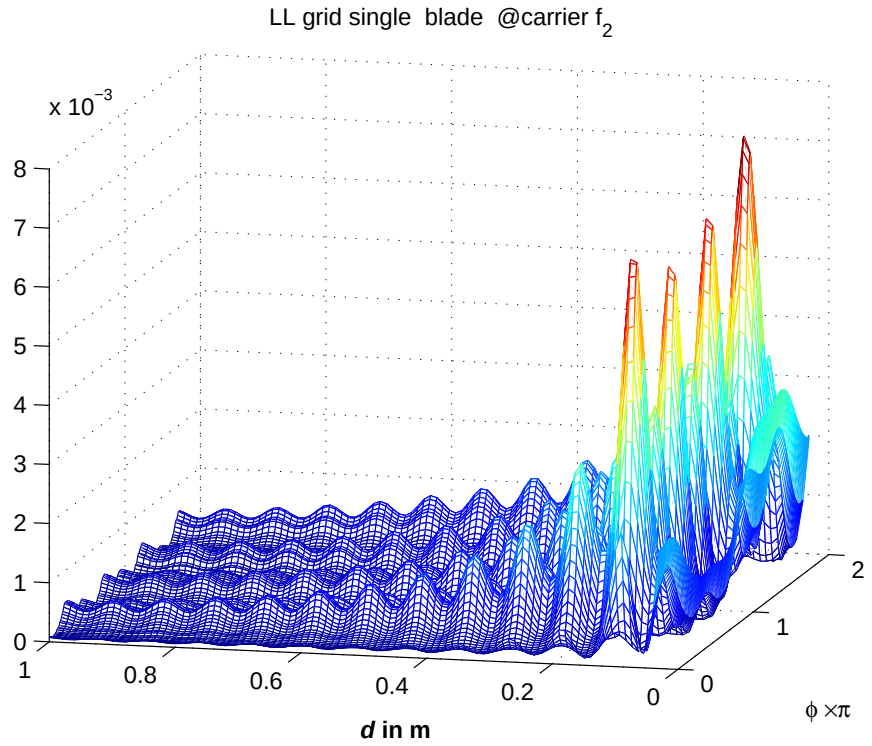

Fig. 8(b). LL grid (0° azimuth) using single blade cost function, for carrier f_2. Four blades are clearly seen. Number of samples used is 1200.

Table I. Range estimates at 0° azimuth. True range is 3m.

Data chunks comprising of 500 samples.	Minimized LLcost (NLS) from 8(a)	Minimized LLcost (IRNLS) from 8(a)	Range estimate (NLS) in meters	Range estimate (IRNLS) in meters
100th sample onwards	-28.7104	-28.9614	3.0046	2.9977
700th Sample onwards	-28.5853	-28.9000	3.0052	2.9985
1400th Sample onwards	-29.6069	-30.0953	3.0132	3.0051

Table II. Range estimates at 60° azimuth. True range is 3m.

Data chunks comprising of 500 samples.	Minimized LLcost (NLS) from (8a)	Minimized LLcost (IRNLS) from 8(a)	Range estimate (NLS) in meters	Range estimate (IRNLS) in meters
100th sample onwards	-31.8872	-31.9728	3.2449	3.2336
700th Sample onwards	-31.9589	-32.1712	3.1552	2.9286
1400th Sample onwards	-31.7151	-31.7550	3.0900	3.087

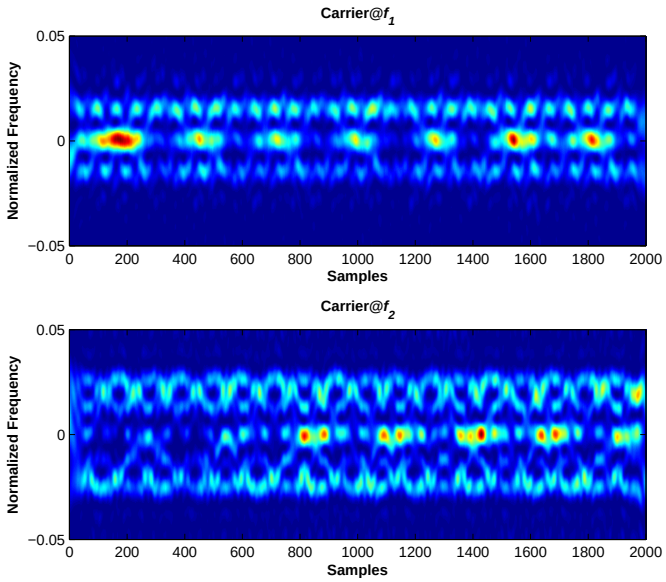

Fig. 9(a). Spectrograms of the measured returns at 60^o azimuth at the two carriers.

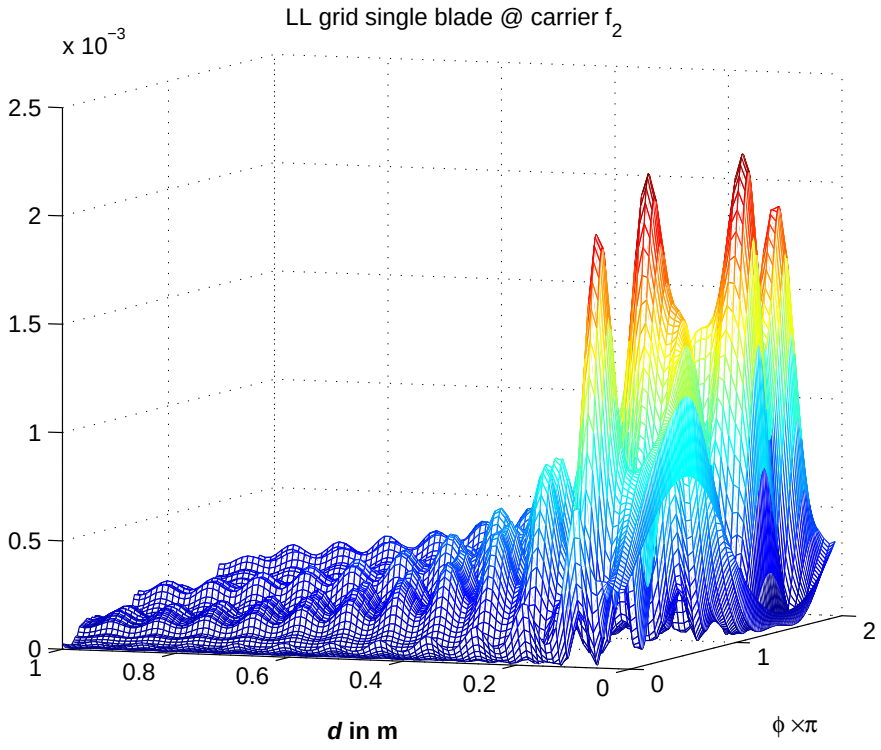

Fig. 9(b). LL grid (60^o azimuth) using single blade cost function, for carrier f_2. Four blades are clearly seen. Number of samples used is 1200.